High temperature GaAs X-ray detectors

Article (Published Version)

High temperature GaAs X-ray detectors

G. Lioliou, M. D. C. Whitaker, and A. M. Barnett

Citation: Journal of Applied Physics **122**, 244506 (2017);
View online: https://doi.org/10.1063/1.5005878
View Table of Contents: http://aip.scitation.org/toc/jap/122/24
Published by the American Institute of Physics

High temperature GaAs X-ray detectors

G. Lioliou,[a] M. D. C. Whitaker, and A. M. Barnett
Space Research Group, School of Engineering and Informatics, University of Sussex, Falmer, Brighton BN1 9QT, United Kingdom

(Received 20 September 2017; accepted 4 December 2017; published online 27 December 2017)

Two GaAs p^+-i-n^+ mesa X-ray photodiodes were characterized for their electrical and photon counting X-ray spectroscopic performance over the temperature range of 100 °C to –20 °C. The devices had 10 μm thick i layers with different diameters: 200 μm (D1) and 400 μm (D2). The electrical characterization included dark current and capacitance measurements at internal electric field strengths of up to 50 kV/cm. The determined properties of the two devices were compared with previously reported results that were made with a view to informing the future development of photon counting X-ray spectrometers for harsh environments, e.g., X-ray fluorescence spectroscopy of planetary surfaces in high temperature environments. The best energy resolution obtained (Full Width at Half Maximum at 5.9 keV) decreased from 2.00 keV at 100 °C to 0.66 keV at –20 °C for the spectrometer with D1, and from 2.71 keV at 100 °C to 0.71 keV at –20 °C for the spectrometer with D2. Dielectric noise was found to be the dominant source of noise in the spectra, apart from at high temperatures and long shaping times, where the main source of photopeak broadening was found to be the white parallel noise. https://doi.org/10.1063/1.5005878

I. INTRODUCTION

The favourable attributes of GaAs compared to other semiconductors have led to the continued progressive development of GaAs X-ray detectors suitable for operating at high temperatures (≥20 °C) without cooling and in intense radiation environments. Its relatively wide bandgap (1.42 eV[1]) results in a lower intrinsic carrier concentration, n_i, at a given temperature (10^7 cm^{-3}, at room temperature) compared to semiconductors with narrower bandgaps, such as Si (10^{10} cm^{-3}, at room temperature).[2] This has a direct effect on the thermally stimulated leakage current and, hence, on the energy resolution achievable with the X-ray spectrometer.[3,4] Furthermore, a higher quantum detection efficiency per unit thickness can be achieved with GaAs due to its greater linear X-ray attenuation coefficients,[5] compared to Si. Additionally, GaAs has been shown to be radiation damage resistant to γ-rays,[6,7] fast neutrons,[8] and high energy electrons.[9] Compared to Si, GaAs is more radiation hard for γ-rays, electrons, low energy protons (<50 MeV[10]), and neutrons; however, it should be noted that results have been reported showing that GaAs is less radiation hard than Si for high energy hadrons.[11]

Owens *et al.*[12,13] reported a planar 5 × 5 GaAs p^+-i-n^+ diode array structure, with a 40 μm epilayer and Au/Pt/Ti Schottky contacts at the p^+ layer, which had low dark current densities (<6 nA/cm^2) and the best energy resolution (0.266 keV Full Width at Half Maximum, *FWHM*, at 5.9 keV, at room temperature) reported to date for GaAs X-ray diodes. Later devices with similar structure but thicker epilayer (325 μm) had an energy resolution of 0.300 keV *FWHM* at 5.9 keV, at room temperature.[14] However, it should be noted that such good energy resolutions have not since been replicated by other researchers (Refs. 12 and 14 had multiple authors in common) despite significant international effort. Work has also been conducted on GaAs p^+-i-n^+ mesa X-ray photodiodes with increasing i layer thickness. The energy resolution of GaAs p^+-i-n^+ mesa X-ray photodiodes with 2 μm thick i layers was investigated as a function of temperature; it was found to broaden from 0.8 keV at room temperature to 1.5 keV at 80 °C.[15] GaAs p^+-i-n^+ mesa X-ray photodiodes with 3 μm i layer thickness were studied at 33 °C over the energy range 4.95 keV to 59.5 keV; the energy resolution (*FWHM*) was found to range from 0.78 keV to 0.95 keV for a 200 μm diameter device and from 1.08 keV to 1.33 keV for a 400 μm diameter device.[16] Systematic study of fabrication techniques for GaAs p^+-i-n^+ mesa X-ray photodiodes with 7 μm i layer thickness investigated the effects of wet chemical etchants and etch depths on the dark currents of such devices; a fully etched 400 μm diameter diode had a *FWHM* at 5.9 keV of 1 keV, at room temperature.[17] The energy resolution (*FWHM* at 5.9 keV) as a function of temperature of similar GaAs p^+-i-n^+ mesa X-ray photodiodes with 7 μm i layer thickness was studied and found to increase from 0.73 keV at 0 °C to 0.84 keV at 60 °C.[18] Results characterizing GaAs p^+-i-n^+ mesa X-ray photodiodes with 10 μm i layer thickness at room temperature showed an energy resolution of 0.625 keV (200 μm diameter device) and 0.740 keV (diameter device) at 5.9 keV, at room temperature.[19]

Here, results across the temperature range of 100 °C to –20 °C are presented for two GaAs p^+-i-n^+ mesa X-ray photodiodes with 10 μm i layer thickness and different (200 μm and 400 μm) diameters. The devices were electrically characterized, and their key parameters were calculated as a

[a]Author to whom correspondence should be addressed: G.Lioliou@sussex.ac.uk. Tel.: +44 (0) 1273 872568.

function of temperature. X-ray spectra were accumulated using the devices connected to a custom-made charge-sensitive preamplifier and illuminated by an ^{55}Fe radioisotope X-ray source. The photodiodes and preamplifier were operated uncooled at temperatures from 100 °C (the highest ever reported temperature for a GaAs X-ray detector) to –20 °C. The different noise contributions were detangled, and the results were compared with previous reports.

II. DEVICE STRUCTURE

The GaAs p^+-i-n^+ mesa photodiodes were grown and fabricated to the authors' specifications at the EPSRC National Epitaxy Facility, Sheffield, UK. GaAs epilayers were grown on a commercial GaAs n^+ substrate by metalorganic vapor phase epitaxy. The unintentionally doped i layer had a thickness of 10 μm. The p^+ layer, having a thickness of 0.5 μm, was doped with C at a doping density of 2×10^{18} cm^{-3}. The n^+ layer, having a thickness of 1 μm, was doped with Si at a doping density of 2×10^{18} cm^{-3}. Mesa diodes (fully etched) with diameters of 200 μm and 400 μm were wet chemically etched using a 1:1:1 H_3PO_4:H_2O_2:H_2O solution followed by 10 s in a 1:8:80 H_2SO_4:H_2O_2:H_2O solution. The top Ohmic contact, consisting of 20 nm of Ti and 200 nm of Au, covered 45% of the surface of the 200 μm diameter devices and the 33% of the 400 μm diameter devices. The rear Ohmic contact consisted of 20 nm of InGe and 200 nm of Au. A summary of the GaAs wafer structure can be seen in Table I. The GaAs devices were unpassivated. The quantum detection efficiency of the photodiodes at the X-ray energy range up to 30 keV was calculated and can be seen in Fig. 1; as a conservative assumption, the whole of the p^+ layer was assumed to be inactive, with the active region of the photodiode being solely the i layer. For comparison purposes, the quantum detection efficiency of the devices with both the p^+ and the i layer being active was also calculated, as shown in Fig. 1. The devices were packaged in TO-5 cans.

III. ELECTRICAL CHARACTERIZATION

Two GaAs devices (D1 and D2) of different diameters (200 μm and 400 μm, respectively) were electrically characterized across the temperature range of 100 °C to –20 °C. Dark current and capacitance measurements as functions of forward (0 V to 1 V) and reverse (0 V to –50 V) bias are presented below.

TABLE I. Layers structure of the GaAs p^+-i-n^+ wafer.

Material	Type	Thickness (nm)	Doping density (cm^{-3})
GaAs	p^+	10	1×10^{19}
GaAs	p^+	500	2×10^{18}
GaAs	i	10 000	Undoped
GaAs	n^+	1000	2×10^{18}
GaAs	n^+ (substrate)		

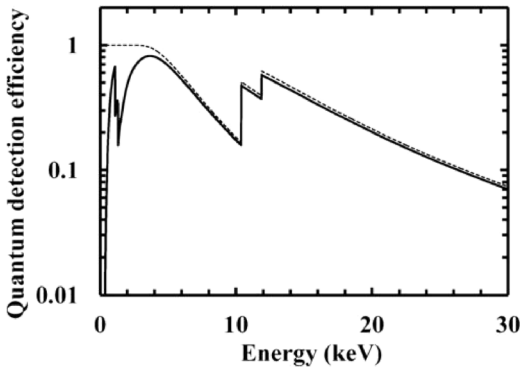

FIG. 1. Calculated X-ray quantum detection efficiency of the GaAs p^+-i-n^+ mesa photodiodes (10 μm i layer thick) with the p^+ layer (0.5 μm) considered dead (solid line) and active (dotted line), as a function of X-ray photon energy.

A. Dark current measurements

Dark currents as functions of applied forward and reverse bias of both packaged diodes, D1 and D2, were measured using a Keithley 6487 Picoammeter/Voltage Source. The diodes were installed inside a TAS Micro MT climatic cabinet for temperature control. The temperature was initially set to 100 °C and decreased to –20 °C, in 20 °C steps. To ensure thermal equilibrium, the diodes were left to stabilize at each temperature for 30 min before the measurements were started at each temperature. Dry N_2 was continually flowing into the climatic cabinet throughout the measurements to maintain a dry (<5% relative humidity) environment. The leakage current associated with each device's TO-5 package was also measured as a function of bias and temperature. The measured dark current as a function of applied forward bias and temperature for both packaged diodes, D1 and D2, with the leakage current of the package subtracted, can be seen in Fig. 2.

The current, I_F, as a function of applied forward bias, V_{AF}, (for $V_{AF} > kT/q$) which is equal to the voltage drop across the diode, $V_D = V_{AF}$, for a p-n diode can be approximated to

$$I_F = I_{sat} e^{qV_D/nkT} = I_{diff} + I_{rec}, \tag{1}$$

where I_{sat} is the saturation current, q is the charge of an electron, n is the ideality factor used to take into account any deviations of a real diode from an ideal diode, k is the Boltzmann constant, and T is the temperature in K.[20] The current, I_F, can be approximated to the sum of the diffusion current, I_{diff}, and the recombination current, I_{rec}. The temperature dependence of the diffusion current, I_{diff}, and the recombination current, I_{rec}, is

$$I_{diff} \propto n_i e^{qV_D/2kT} \tag{2}$$

and

$$I_{rec} \propto n_i^2 e^{qV_D/kT}, \tag{3}$$

respectively, where n_i is the intrinsic carrier concentration of the semiconductor at a given temperature. The saturation

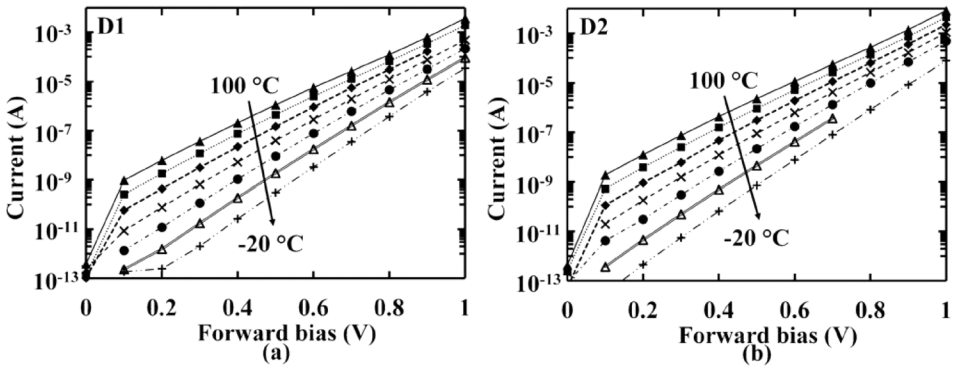

FIG. 2. Current as a function of applied forward bias for the GaAs p^+-i-n^+ mesa photodiode (a) D1 and (b) D2 in the temperature range 100 °C to –20 °C. The data points have been joined with lines for clarity.

current, I_{sat}, and ideality factor, n, can be both extracted from the semi-logarithmic current, I_F, as a function of applied forward bias, V_{AF}, plot. The ideality factor, n, equals 1 when the diffusion current, I_{diff}, dominates [Eq. (3)] and 2 when the recombination current, I_{rec}, dominates [Eq. (2)].[20] It lies between 1 and 2 when both currents are comparable. The saturation current was found to vary from 240 pA ± 30 pA at 100 °C to 1.8 fA ± 0.2 fA at –20 °C for D1, and from 480 pA ± 50 pA at 100 °C to 3.8 fA ± 0.3 fA at –20 °C for D2. The calculated ideality factor as a function of temperature for both diodes can be seen in Fig. 3. The uncertainties in the saturation current and the ideality factor were related to the standard deviation of the gradient and the intercept point with the current, I_F, at 0 V applied forward bias, of the line of best fit calculated for the semi-logarithmic current, I_F, as a function of applied forward bias, V_{AF}, plot using linear least squares fitting.

For D1, the ideality factor, n, improved from (1.91 ± 0.02) at –20 °C to (1.84 ± 0.02) at 0 °C and then remained stable, within uncertainties, up to 100 °C. The ideality factor improved from (1.90 ± 0.01) at –20 °C to (1.86 ± 0.02) at 20 °C for D2 and remained stable, within uncertainties, up to 100 °C. This improvement was attributed to the reduction of the recombination current and the increase of the diffusion current as the temperature increased.[20] Although the ideality factor, n, was temperature-dependent, its small increase as the temperature decreased from 100 °C to –20 °C was not sufficient to indicate the significant contribution of tunnelling in the conduction process.[21]

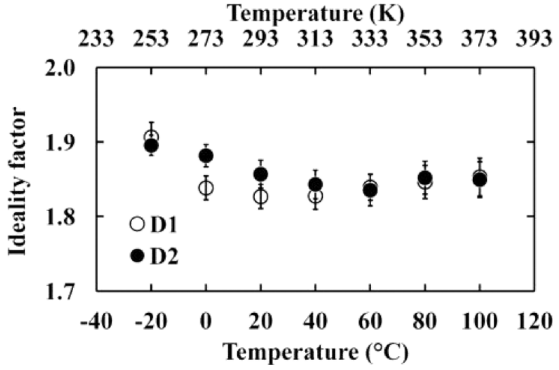

FIG. 3. Ideality factor extracted from the measured current as a function of applied forward bias for the GaAs p^+-i-n^+ mesa photodiode D1 (open circles) and D2 (filled circles) in the temperature range of 100 °C to –20 °C. The error bars were calculated propagating the standard deviation of the gradient of the line of best fit of the measured current as a function of applied forward bias.

The leakage current, I_R, as a function of reverse applied bias, V_{AR}, of the two GaAs p^+-i-n^+ mesa photodiodes, with the leakage current of the package subtracted, is shown in Fig. 4. The leakage current of D1 at –50 V reverse bias was found to decrease from 1.615 nA ± 0.007 nA at 100 °C to a current (0.1 pA) smaller than its uncertainty associated with the measurement (±0.4 pA) at -20 °C. The leakage current of D2 at –50 V reverse bias was found to decrease from 2.43 nA ± 0.01 nA at 100 °C to a current (0.2 pA) which was again smaller than the uncertainty associated with the measurement (±0.4 pA) at –20 °C. The leakage current density, J_R, at –50 V reverse bias (50 kV/cm internal electric field) of both devices as a function of temperature can be seen in Fig. 5. The leakage current density of both devices showed an exponential decrease with a constant factor, 0.08, as the temperature decreased from 100 °C to –20 °C. It should be noted that the lines of best fit were calculated using linear least squares fitting, excluding the current measurements at –20 °C because the uncertainties associated with data at that temperature were greater than the values themselves. The leakage current was found to be not to scale with the junction area: the 400 μm diameter device (D2) had lower leakage current density than the 200 μm diameter device (D1) at all temperatures (Fig. 5). This suggested that the surface leakage current was not negligible. Surface passivation of GaAs has been previously studied and shown to suppress, and even eliminate, the surface states, which are formed by segregated arsenic atoms via oxidation, giving rise to surface leakage current.[22–24] Both GaAs p^+-i-n^+ diodes showed leakage current densities comparable with other high quality GaAs p^+-i-n^+ diodes. Leakage current densities of 5.14 μA/cm^2 ± 0.02 μA/cm^2 (for D1) and 1.937 μA/cm^2 ± 0.008 μA/cm^2 (for D2) were recorded at the maximum investigated temperature (100 °C) and internal electric field (50 kV/cm).

Previously reported thinner (7 μm) GaAs mesa p^+-i-n^+ photodiodes had leakage current densities of 2 μA/cm^2 and 0.5 μA/cm^2, at 100 °C and an applied electric field of 21.4 kV/cm.[18] A GaAs pixel p^+-i-n^+ mesa photodiode detector reported by Bertuccio *et al.*[25] had a leakage current density of 92 nA/cm^2 at 30 °C and 33 kV/cm applied electric field. For comparison purposes, interpolating the leakage current density of D1 and D2 at 30 °C (Fig. 5) gives 15 nA/cm^2 and 6 nA/cm^2 at 50 kV/cm internal electric field, for D1 and D2, respectively.

The reverse leakage current, I_R, (and the current density, J_R) of a p^+-i-n^+ junction can be approximated to the sum of

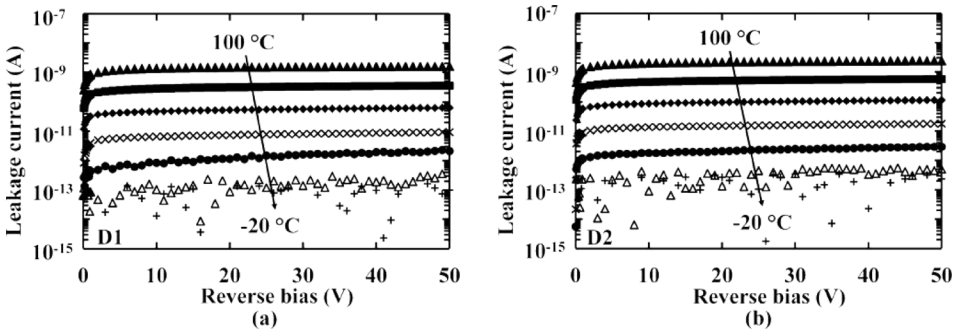

FIG. 4. Leakage current as a function of applied reverse bias for the GaAs p^+-i-n^+ mesa photodiode (a) D1 and (b) D2 in the temperature range of 100 °C to –20 °C.

the diffusion current, I_{diff}, and the generation current, I_{gen}.[20] The diffusion current and the generation current have a different dependency upon the intrinsic carrier concentration, n_i, the diffusion current scales with n_i^2 whereas the generation current scales with n_i. Also

$$n_i \propto e^{-E_G/2kT} \tag{4}$$

and

$$n_i^2 \propto e^{-E_G/kT}, \tag{5}$$

where E_G is the bandgap of the semiconductor (= 1.42 eV for GaAs[1]). Hence, a plot of ln(J_R) as a function of 1/kT would yield a straight line whose gradient would determine the dominant current mechanism. The logarithmic of leakage current density, ln(J_R), at 50 kV/cm as a function of 1/kT graph for both D1 and D2, along with the fitted lines using linear least squares fitting (excluding the measurements at –20 °C, since their uncertainties were greater than the values themselves) can be seen in Fig. 6. The gradients of the fitted lines were found to be equal to $-E_G/2$ (–0.74 eV ± 0.3 eV for D1 and –0.75 eV ± 0.2 eV for D2), suggesting that the prevailing conduction process was generation.

B. Capacitance measurements

Capacitances as functions of applied forward and reverse bias were measured for each diode under dark conditions, using an HP 4275A Multi Frequency LCR meter, with a 50 mV rms magnitude test signal and a 1 MHz frequency. The diodes were installed inside a TAS Micro MT climatic cabinet for temperature control, as per the dark current measurements.

Each diode was measured when packaged, and hence the measured capacitance, C_{Dmeas}, included the capacitance of the package, C_{pack}, as well as the capacitance of the diode, C_D. Thus the capacitance of the packages used was also measured as a function of the same bias and temperature range as diodes D1 and D2 and subtracted from the measured capacitance, C_{Dmeas}, to deduce the diode capacitance, C_D. The uncertainty associated with a single capacitance measurement (C_{Dmeas} or C_{pack}) was estimated to be ± 0.03 pF, whereas the uncertainty for all the reported values for the diode capacitance, C_D (= C_{Dmeas} – C_{pack}), was estimated to be ± 0.04 pF. However, it should be noted that the reported capacitance variations with temperature, $C_D(T)$, for each diode resulted from a single set of measurements taken at the same conditions (i.e., only the temperature was varied and no interconnections were changed), and hence, the associated uncertainty was estimated to range from ± 0.005 pF to ± 0.013 pF, being proportional to the value of the corresponding measured capacitance, C_{Dmeas}. The diode capacitance, C_D, as a function of applied forward bias in the temperature range of 100 °C to –20 °C for both diodes, D1 and D2, can be seen in Fig. 7.

The capacitance of each GaAs p^+-i-n^+ mesa photodiode decreased at each applied forward bias, as the temperature was decreased from 100 °C to –20 °C. The capacitance decreased from 4.368 pF ± 0.008 pF at 100 °C to

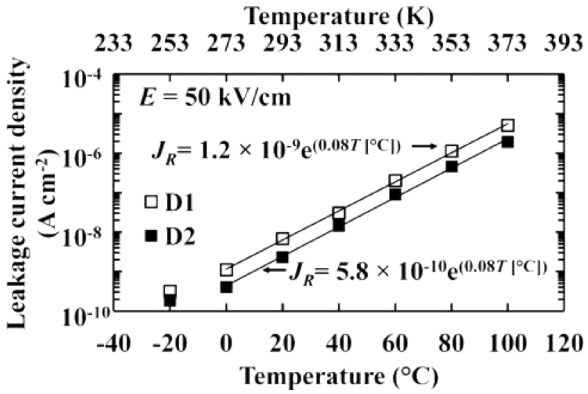

FIG. 5. Measured leakage current density as a function of temperature at 50 kV/cm internal electric field for the GaAs p^+-i-n^+ mesa photodiode D1 (open squares) and D2 (filled squares). The line of best fit, as calculated with the linear least squares fitting, at the temperature range of 100 °C to 0 °C can also be seen.

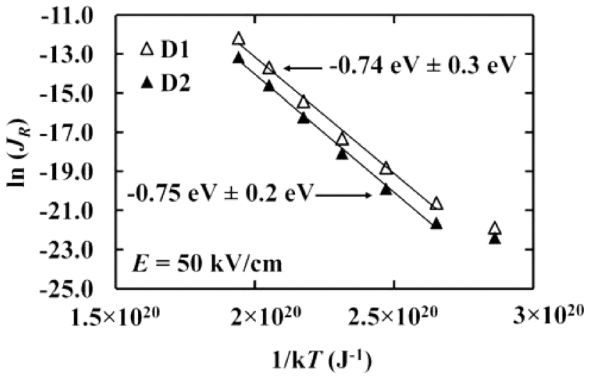

FIG. 6. Ln(J_R) as a function of 1/kT (in units of joules^{-1}) for the GaAs p^+-i-n^+ mesa photodiode D1 (open triangles) and D2 (filled triangles). The lines of best fit, as determined by linear least squares fitting, across the temperature range of 100 °C to 0 °C, and the gradients of the lines (–0.74 eV ± 0.3 eV for D1; –0.75 eV ± 0.2 eV for D2) can also be seen.

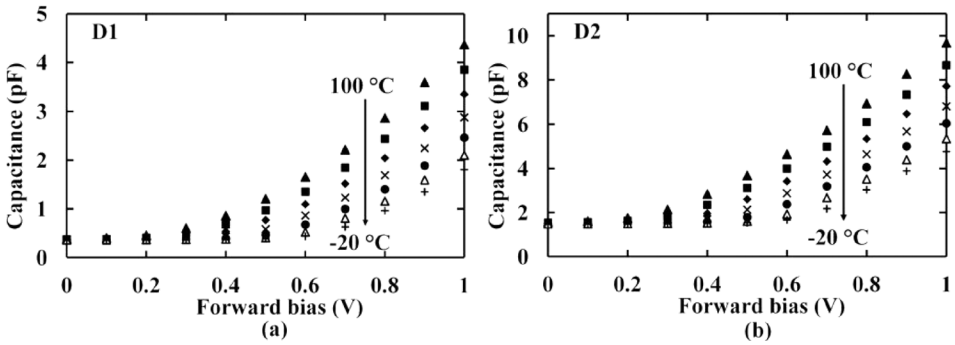

FIG. 7. Capacitance as a function of applied forward bias for the GaAs p^+-i-n^+ mesa photodiodes (a) D1 and (b) D2 in the temperature range of 100 °C to –20 °C.

1.806 pF ± 0.006 pF at –20 °C for D1, and from 9.679 pF ± 0.014 pF at 100 °C to 4.765 pF ± 0.009 pF at –20 °C for D2, at 1 V forward bias. The diffusion capacitance, C_{diff}, significantly contributed to the diode capacitance, C_D, at forward biases. The diffusion capacitance, C_{diff}, arises due to the rearrangement of the minority carrier density and is directly proportional to the forward current, I_F.[20] The observed dependency of the forward capacitance with temperature (Fig. 7) was thus attributed to the same temperature dependence of the forward current with temperature (Fig. 2).

The diode capacitance, C_D, as a function of applied reverse bias in the temperature range 100 °C to –20 °C for both diodes, D1 and D2, can be seen in Fig. 8. The depletion layer capacitance, C_{DL}, defined the reverse biased diode capacitance. The depletion layer capacitance of D1 decreased from 0.388 pF ± 0.005 pF at 100 °C to 0.357 pF ± 0.005 pF at –20 °C at 0 V, and from 0.344 pF ± 0.005 pF at 100 °C to 0.334 pF ± 0.005 pF at –20 °C, at –50 V reverse bias. Similarly, the depletion layer capacitance of D2 decreased from 1.576 pF ± 0.006 pF at 100 °C to 1.471 pF ± 0.006 pF at –20 °C at 0 V, and from 1.416 pF ± 0.006 pF at 100 °C to 1.396 pF ± 0.006 pF at –20 °C, at –50 V reverse bias. For both diodes, the most significant capacitance change with temperature occurred at low applied reverse bias. It should be noted here that the measured capacitances at –50 V reverse bias of both D1 and D2 (0.344 pF at 100 °C and 0.357 pF at –20 °C for D1; 1.416 pF at 100 °C; and 1.396 pF at –20 °C for D2) were very close to the calculated capacitance values, assuming the devices may be approximated as parallel plate capacitors (0.356 pF for D1 and 1.424 pF for D2).

The measured depletion layer capacitance (Fig. 8) was used to calculate the depletion layer width, W_D, of both diodes as a function of applied reverse bias, at all the investigated temperatures.[18] The calculated depletion layer capacitance at 100 °C and –20 °C of both diodes can be seen in Fig. 9. The depletion layer width was found to increase for D1 by 0.8 μm ± 0.2 μm (from 9.2 μm ± 0.1 μm at 100 °C to 10.0 μm ± 0.1 μm at –20 °C), and for D2 by 0.65 μm ± 0.05 μm (from 9.10 μm ± 0.03 μm at 100 °C to 9.76 μm ± 0.04 μm at –20 °C), as the temperature decreased from 100 °C to –20 °C at zero applied bias. A smaller increase in the depletion layer width as the temperature decreased from 100 °C to –20 °C was found at –50 V reverse bias compared to 0 V; it increased for D1 by 0.3 μm ± 0.2 μm (from 10.4 μm ± 0.1 μm at 100 °C to 10.7 μm ± 0.2 μm at –20 °C), and for D2 by 0.14 μm ± 0.06 μm (from 10.13 μm ± 0.04 μm at 100 °C to 10.28 μm ± 0.04 μm at –20 °C). The above observation was explained by the possible presence of a thin region around the depletion layer with non-ionized dopants at low temperatures, which were progressively ionized at high temperatures, thus limiting the extension of the depletion layer.[26]

The depletion layer of a p^+-i-n^+ diode can extend throughout the i layer and in some circumstances penetrate into the p^+ and/or n^+ layers.[27] For highly doped (low resistivity) p^+ and n^+ regions, as is the case for the reported diodes, the maximum depletion layer is set by the i layer thickness. Hence, it can be said that the i layer thicknesses of D1 and D2 were 10 μm ± 1 μm and 10.3 μm ± 0.3 μm, respectively. The uncertainty of the i layer thickness of each diode was associated with the uncertainty of the diode capacitance, C_D (± 0.04 pF).

The effective doping concentration of the intrinsic layer, N_{eff}, of a p^+-i-n^+ diode can be extracted from capacitance measurements as functions of applied reverse bias, using the differential capacitance profiling method.[28] The effective doping concentration can be approximated to the concentration of the majority carriers in the intrinsic layer, but both can be different from the doping density.[29] When the doping profile of the i layer does not have a sharp gradient (spatial

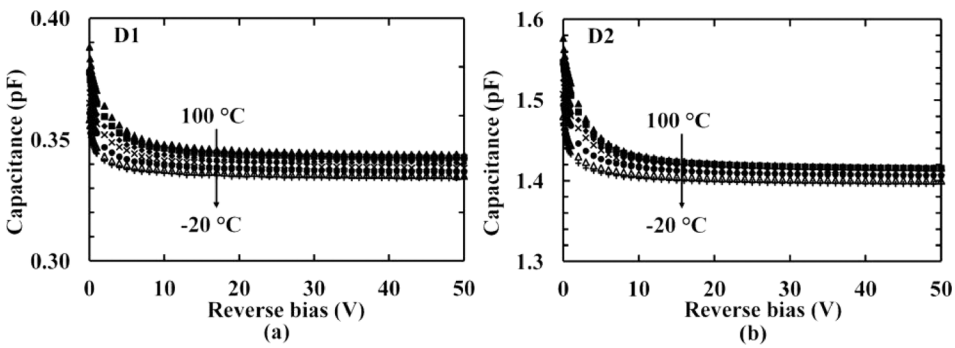

FIG. 8. Capacitance as a function of applied reverse bias for the GaAs p^+-i-n^+ mesa photodiodes (a) D1 and (b) D2 in the temperature range of 100 °C to –20 °C.

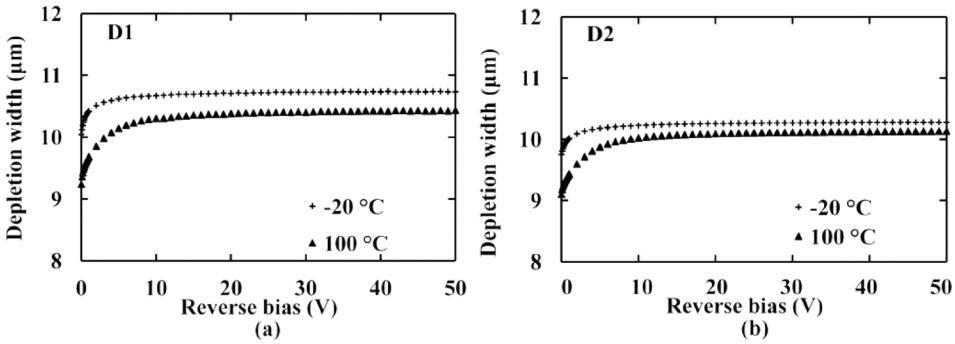

FIG. 9. Calculated depletion layer width for the GaAs p^+-i-n^+ mesa photodiodes (a) D1 and (b) D2 at 100 °C (filled triangles) and –20 °C (+ symbols).

variation over distances less than the Debye length), the extracted carrier concentration follows the doping profile. The Debye length is a function of the semiconductor material, its doping density and the temperature.[20] It was calculated for GaAs with a doping concentration of $10^{14}\,cm^{-3}$ to range between 0.4 μm (at –20 °C) and 0.5 μm (at 100 °C). The currently reported devices were almost fully depleted) at all investigated temperatures, even at no applied bias. Thus, the effective doping concentration could be calculated at distances below the p^+-i junction of >9 μm only, rather than the whole i layer. The effective doping profiles of both diodes as calculated from capacitance measurements, at 100 °C and –20 °C, can be seen in Fig. 10.

The effective doping concentration of D1 was found to increase from $8.2 \times 10^{13}\,cm^{-3}$ at 9.3 μm ± 0.1 μm below the p^+-i junction to $5 \times 10^{16}\,cm^{-3}$ at the i-n^+ interface at 100 °C, and from $9 \times 10^{13}\,cm^{-3}$ at 10.1 μm ± 0.1 μm below the p^+-i junction to $4 \times 10^{16}\,cm^{-3}$ at the i-n^+ interface at –20 °C. Similarly, the effective doping concentration of D2 was found to increase from $1.22 \times 10^{14}\,cm^{-3}$ at 9.19 μm ± 0.03 μm below the p^+-i junction to $2 \times 10^{17}\,cm^{-3}$ at the i-n^+ interface at 100 °C, and from $1.54 \times 10^{14}\,cm^{-3}$ at 9.80 μm ± 0.04 μm below the p^+-i junction to $2 \times 10^{17}\,cm^{-3}$ at the i-n^+ interface at −20 °C. The difference between the effective doping concentration of both diodes, D1 and D2, at 100 °C and –20 °C was attributed to non-ionized dopants in a layer at the i-n^+ interface at low temperatures, which were progressively ionized at high temperatures and which limited the extension of the depletion layer.

IV. X-RAY SPECTROSCOPY

The X-ray detection performance of the GaAs p^+-i-n^+ mesa photodiode detectors, D1 and D2, was characterized as a function of temperature. ^{55}Fe X-ray spectra were obtained using the X-ray spectrometer S1 (employing detector D1) and S2 (employing detector D2). Both spectrometers, S1 and S2, had the same front-end electronics (charge-sensitive preamplifier); only the detector was different between the X-ray spectrometers S1 and S2. First, the obtained ^{55}Fe X-ray spectra at the temperature range of 100 °C to –20 °C are presented, followed by noise analysis of the resultant spectrometer system.

A. ^{55}Fe X-ray spectra measurements

An ^{55}Fe radioisotope X-ray source (activity of 175 MBq) was positioned 3 mm above the top of each device. The 200 μm diameter device, D1, was directly illuminated with the radioisotope X-ray source, but the 400 μm diameter device, D2, had a 300 μm thick PTFE attenuator placed between the ^{55}Fe radioisotope X-ray source and the photodiode to reduce the count rate to similar to that seen with D1. Each device was connected to a custom-made, single-channel, charge-sensitive preamplifier employing a similar feedback-resistorless design as Ref. 30. A Vishay 2N4416A Si JFET was used as the input transistor.[31] The detector and preamplifier were installed inside a TAS Micro MT climatic cabinet throughout the measurements for temperature control. The temperature was initially set to 100 °C and decreased to –20 °C, in 20 °C steps, with the same experimental protocol as was used for the electrical characterisation. The output signal of the preamplifier was shaped using an Ortec 572A shaping amplifier which was further connected to an Ortec EASYMCA 8k multi-channel analyser (MCA) for digitization.

^{55}Fe X-ray spectra were accumulated at each temperature at 0 V, –5 V, –10 V, –15 V, and –20 V reverse bias. The

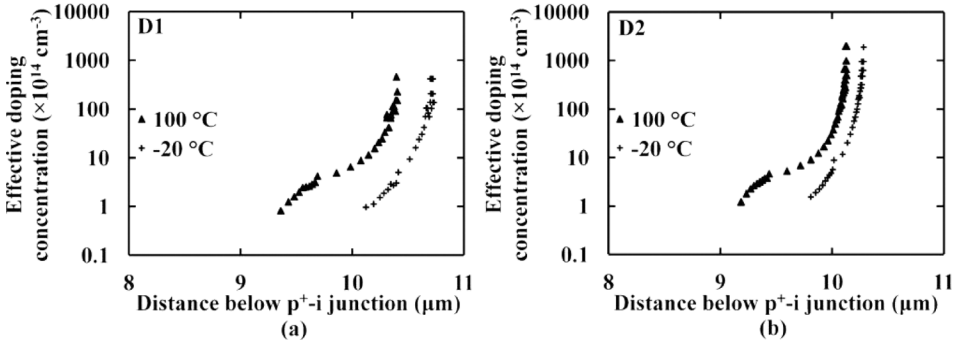

FIG. 10. Calculated effective doping concentration for the GaAs p^+-i-n^+ mesa photodiodes (a) D1 and (b) D2 at 100 °C (filled triangles) and –20 °C (+ symbols).

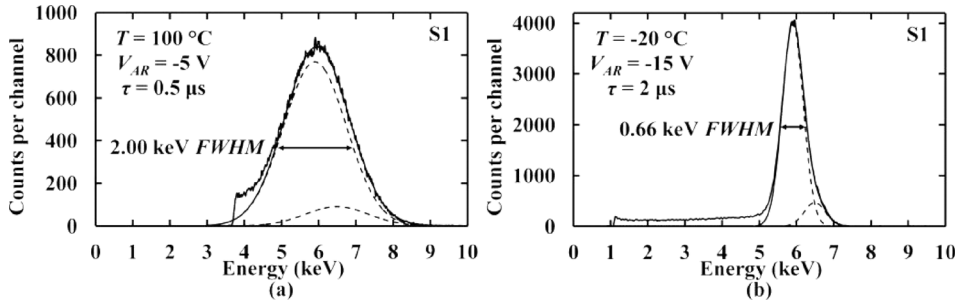

FIG. 11. ^{55}Fe X-ray spectra accumulated with the GaAs p^+-i-n^+ mesa photodiode based spectrometer S1 at (a) 100 °C (–5 V reverse bias and 0.5 μs shaping time) and (b) –20 °C (–15 V reverse bias and 2 μs shaping time). The fitted Mn Kα and Kβ peaks (dashed lines) along with the combined Gaussian peak fit (solid line) can also be seen. The low-energy cut-off threshold in (a) was set at a value greater than necessary due to operator error, thus the tail of the so-called zero energy noise peak cannot be seen.

shaping time, τ, was varied; spectra were accumulated for τ = 0.5 μs, 1 μs, 2 μs, 3 μs, 6 μs, and 10 μs at each applied reverse bias. The live time limit of each spectrum was 120 s. The photopeak detected from the ^{55}Fe radioisotope X-ray source in each case was the combination of the characteristic Mn Kα (5.9 keV) and Mn Kβ (6.49 keV) lines the source.[32] Gaussians were fitted to the peak taking into account the relative emission ratio[33] and the relative efficiency of the detector (Fig. 1) at 5.9 keV and 6.49 keV. The differing attenuation of the 5.9 keV and 6.49 keV X-rays through the 300 μm thick PTFE attenuator was also taken into account for D2. The positions of the zero energy noise peak and the Mn Kα peak were used to energy calibrate the spectra. The obtained spectra with the best energy resolution (smallest *FWHM*) at the highest (100 °C) and lowest (–20 °C) investigated temperatures for both X-ray spectrometers, S1 and S2, employing the detectors D1 and D2, respectively, can be seen in Figs. 11 and 12.

The low energy tailing seen in Figs. 11 and 12 was attributed to partial charge collection of charge created in the non-active layers of the device. The valley-to-peak (*V*/*P*) ratio was calculated for both X-ray spectrometers, S1 and S2, in the temperature range 80 °C to –20 °C (the low energy tail of the photopeak was partly overlapped by the tail of the zero energy noise peak at 100 °C) from the ratio between counts at 3 keV and counts at 5.9 keV. The *V*/*P* ratio was found to be a function of both shaping time and temperature, and it broadly followed the *FHWM* trend. The best V/P ratio at each temperature improved from 0.07 at 80 °C to 0.03 at –20 °C, for both spectrometers. The *FWHM* at 5.9 keV of X-ray spectrometer S1 was better (smaller) than that of S2 at all investigated temperatures. A comparison between the best measured *FWHM* at 5.9 keV for each spectrometer at each temperature can be seen in Fig. 13. The optimum reverse bias and shaping time was found to vary across the investigated temperature range for both diodes, and it can be seen in Table II. The *FWHM* decreased as the temperature decreased: for S1 the *FWHM* at 5.9 keV reduced from 2.00 keV at 100 °C (–5 V reverse bias and 0.5 μs shaping time) to 0.66 keV at –20 °C (–15 V reverse bias and 2 μs shaping time). Similarly for S2, the *FWHM* at 5.9 keV reduced from 2.71 keV at 100 °C (–5 V reverse bias and 0.5 μs shaping time) to 0.71 keV at –20 °C (–15 V reverse bias and 6 μs shaping time). The best energy resolutions at 20 °C were 0.69 keV and 0.73 keV for the S1 and S2 spectrometers, respectively. Discussion and explanation of these results are presented in Sec. IV B.

B. Noise analysis

The energy resolution of a non-avalanche photodiode spectrometer is commonly defined by the quadratic sum of three independent terms; Fano noise, incomplete charge collection noise, and electronic noise.[34] The Fano noise is related to the statistical nature of the ionization process and was calculated to be 0.128 keV at 5.9 keV in GaAs, assuming a Fano factor, *F*, of 0.12[35] and an electron hole pair creation energy, ω, of 4.184 eV.[1] The incomplete charge collection

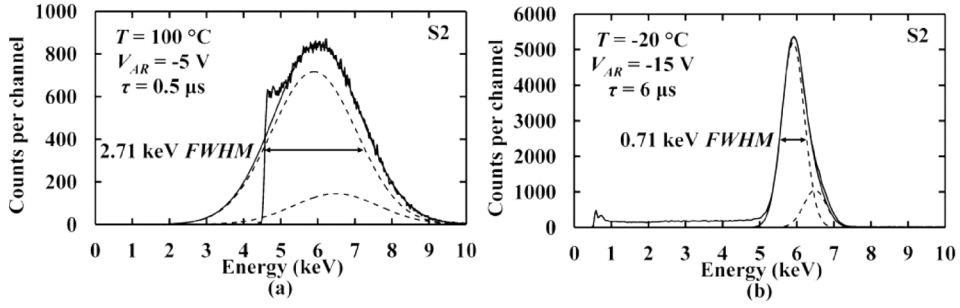

FIG. 12. ^{55}Fe X-ray spectra accumulated with the GaAs p^+-i-n^+ mesa photodiode based spectrometer S2 at (a) 100 °C (–5 V reverse bias and 0.5 μs shaping time) and (b) –20 °C (–15 V reverse bias and 6 μs shaping time). The fitted Mn Kα and Kβ peaks (dashed lines) along with the combined Gaussian peak fit (solid line) can also be seen. The low-energy cut-off threshold in (a) was set at a value greater than necessary due to operator error, thus the tail of the so-called zero energy noise peak cannot be seen.

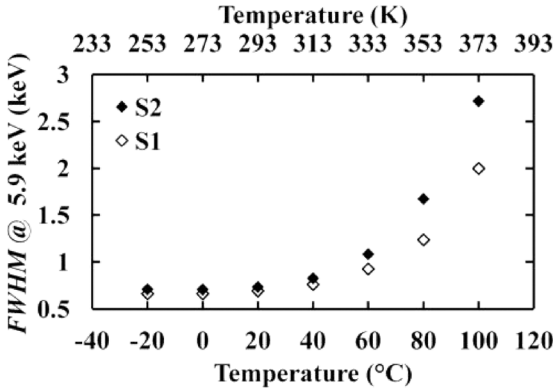

FIG. 13. *FWHM* of 5.9 keV peak as a function of temperature for GaAs p^+-i-n^+ mesa photodiode based spectrometer S1 (open diamonds) and S2 (filled diamonds) at the optimum reverse bias and shaping time.

noise is a result of carrier trapping and recombination due to crystal imperfections;[36] for a photodiode fabricated from the same wafer as the photodiodes presently reported in this article it has been previously found that incomplete charge collection noise was negligible at room temperature even at low reverse biases (–5 V) due to the high quality of the epitaxial material.[19] Electronic noise in semiconductor X-ray spectrometers consists of four main components; white series noise (*WS*) (including the induced gate current noise), white parallel noise (*WP*), 1/*f* noise (1/*f*), and dielectric noise (*DN*).[34]

All the electronic noise components apart from the white series and the white parallel noise are shaping time invariant. The white series noise due to the total capacitance, C_{tot}, at the input of the preamplifier is inversely proportional to the shaping time, and the white parallel noise due to the leakage current of the detector, I_R, and the input JFET is directly proportional to the shaping time. Hence, the experimental values of the *FWHM* as a function of shaping time can be fitted through a multidimensional least squares estimation method to find the noise contributions that are, respectively, shaping time invariant, shaping time inversely proportional, and shaping time directly proportional.[37]

The different noise contributions of the spectrometer were investigated as a function of temperature, in the temperature range of 100 °C to –20 °C, with the detector reverse biased at –5 V for both D1 and D2. The *FWHM* at 5.9 keV as a function of shaping time at each investigated temperature range and –5 V reverse bias using the X-ray spectrometer S1 and S2, can be seen in Fig. 14.

TABLE II. Optimum reverse bias and shaping time for the GaAs p^+-i-n^+ mesa photodiode based spectrometer S1 and S2 at different temperatures.

	S1		S2	
Temperature (°C)	Optimum reverse bias (V)	Optimum shaping time (μs)	Optimum reverse bias (V)	Optimum shaping time (μs)
–20	–15	2	–15	3
0	–10	2	–15	3
20	–5	1	–15	2
40	–5	1	–15	1
60	–5	0.5	–10	0.5
80	–5	0.5	–10	0.5
100	–5	0.5	–5	0.5

There was a substantial improvement in the *FWHM* at 5.9 keV for every 20 °C temperature decrease from 100 °C to 40 °C, with an additional slight improvement in the *FWHM* at 5.9 keV as the temperature further decreased from 40 °C to 20 °C, for both spectrometers S1 and S2 with both diodes, D1 and D2, at –5 V reverse bias. The *FWHM* at 5.9 keV improved at long shaping times ($\geq$3 μs) when the temperature decreased from 20 °C to 0 °C, whereas no improvement was observed in the measured *FWHM* at 5.9 keV for a temperature decrease from 0 °C to –20 °C, for both spectrometers, S1 and S2. Another important observation based on Fig. 14 is the change of the optimum shaping time of the spectrometer with each detector, at different temperatures at –5 V reverse bias. The optimum shaping time lengthened as the temperature decreased from 0.5 μs at 100 °C with both spectrometers, S1 and S2, to 2 μs and 6 μs at –20 °C with S1 and S2, respectively. The optimum shaping time at each temperature (and each applied reverse bias) is defined by the white series and white parallel noise contributions. The minimum (best) *FWHM* is achieved at the shaping time at which the combination (in quadrature) of these contributors is minimised. The presently reported detectors had a more significant reduction in leakage current than in capacitance, as the temperature decreased (Figs. 4 and 8). Hence, it was expected that as the temperature decreased, the reduction in the white parallel noise contribution of the detector would be greater than the reduction in the white series noise contribution of the detector, resulting in the lengthening of the spectrometer's optimum shaping time.

A multidimensional unconstrained nonlinear minimization was applied to the *FWHM* as a function of shaping time

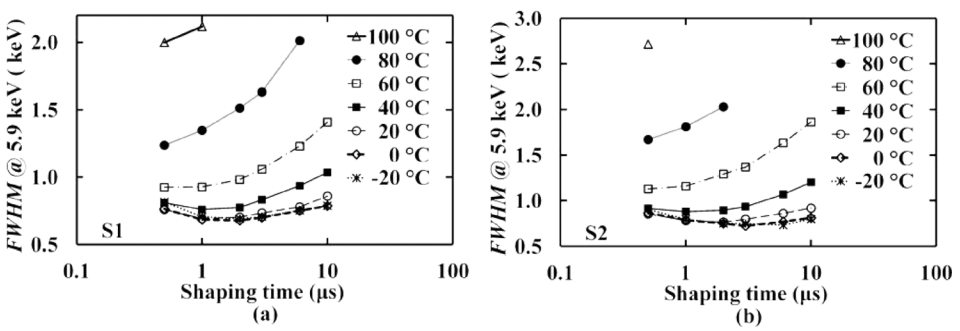

FIG. 14. *FWHM* at 5.9 keV for the GaAs p^+-i-n^+ mesa photodiode based spectrometer (a) S1 and (b) S2 as a function of shaping time at -5 V reverse bias at the temperature range of 100 °C to –20 °C.

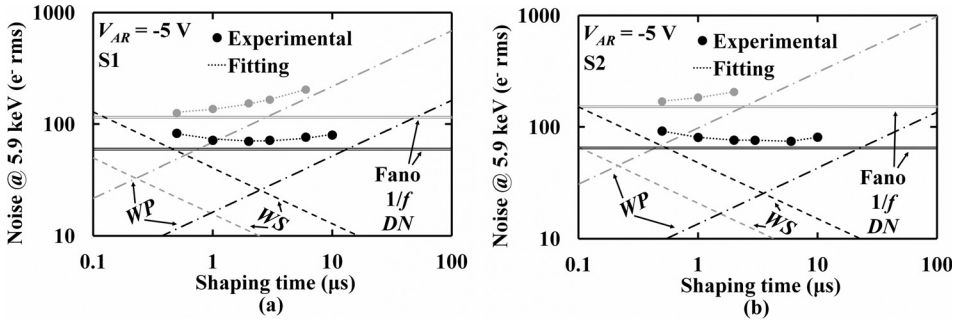

FIG. 15. Equivalent noise charge at 5.9 keV for GaAs p^+-i-n^+ mesa photodiode based spectrometer (a) S1 and (b) S2 as a function of shaping time, at 80 °C (grey symbols) and –20 °C (black symbols) at –5 V reverse bias. The three noise contributions, inversely proportional to shaping time (WS), directly proportional to shaping time (WP), and shaping time invariant (Fano, 1/*f* and DN) have been determined with a multidimensional least squares fitting of the experimental points.

(Fig. 14) for both spectrometers at the temperature range 80 °C to –20 °C, and the fitting at 80 °C and –20 °C can be seen in Fig. 15. The measured *FWHM* at 100 °C was excluded from the following analysis since the number of data points was not sufficient for a multidimensional least squares fitting.

Within the investigated shaping time range (0.5 μs to 10 μs), the dominant source of noise was the dielectric noise, at temperatures $\leq$20 °C. The white parallel noise was the dominant source of noise at temperatures $\geq$40 °C and long shaping times; it dominated over all other noise contributions for shaping times $\geq$3 μs at 80 °C, $\geq$6 μs at 60 °C, and = 10 μs at 40 °C. The white series noise was found to increase with decreased temperature for both spectrometers, S1 and S2, at –5 V reverse bias.

The shaping time invariant contribution, consisting of the Fano noise, the 1/*f* noise, and the dielectric noise (DN), assuming negligible incomplete charge collection noise, was estimated to decrease from 1.14 keV at 80 °C to 0.60 keV at –20 °C for S1, and from 1.50 keV at 80 °C to 0.65 keV at –20 °C for S2. Subtracting in quadrature, the calculated Fano and 1/*f* noise contributions[34] from the total shaping time invariant noise contribution at each temperature for each spectrometer, the dielectric noise, *DN*, was calculated and can be seen in Fig. 16. The dielectric noise was found to vary from 1.13 keV (115 e^- rms) at 80 °C to 0.59 keV (60 e^- rms) at –20 °C for S1, and from 1.50 keV (152 e^- rms) at

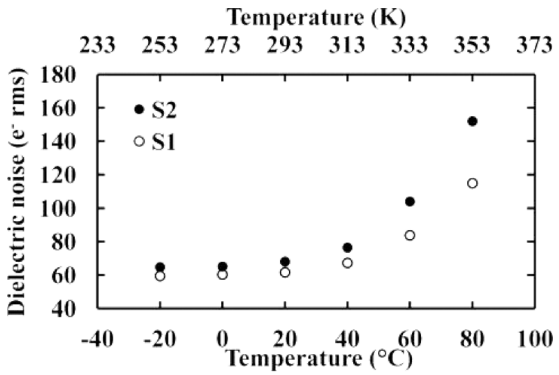

FIG. 16. Dielectric noise for GaAs p^+-i-n^+ mesa photodiode based spectrometer S1 (open circles) and S2 (filled circles) as a function of temperature, as deduced from multidimensional least squares fitting of the measured *FWHM* at 5.9 keV as a function of shaping time, at –5 V reverse bias.

80 °C to 0.64 keV (65 e^- rms) at –20 °C for S2. The dielectric noise of a photodiode X-ray spectrometer arises from any lossy dielectrics at the input of the preamplifier, such as the feedback capacitance, the passivation and packaging of the input JFET, the JFET dielectrics, as well as the detector itself and its packaging.[37–39] The known dependency of the dielectric noise on the temperature[34] explained the reduction of the dielectric noise as the temperature decreased for both spectrometers, S1 and S2. Also, the greater dielectric noise of the X-ray spectrometer S2 (with D2, 400 μm diameter device) compared to the spectrometer S1 (with D1, 200 μm diameter device) was attributed to the higher capacitance of D2 compared to D1, since the dielectric noise is directly proportional to the capacitance of the lossy dielectrics.

The dielectric noise of the GaAs detector and the Si input JFET (not including the JFET's passivation, or the packaging of both the detector and the JFET) is readily estimable.[34] These known dielectric noises at 20 °C, assuming a dissipation factor of 2×10^{-4} for GaAs[40] and 8×10^{-4} for the Si JFET[39] of the X-ray spectrometer S1 and S2, were calculated to total 0.25 keV (25 e^- rms) and 0.26 keV (26 e^- rms) for S1 and S2, respectively. Hence, it was estimated that the additional dielectrics contributed to the *FWHM* at 5.9 keV a total of 0.56 keV (56 e^- rms) and 0.62 keV (63 e^- rms), when S1 and S2 were used, respectively.

The total leakage current of each spectrometer was estimated from the τ proportional contribution of the multidimensional least squares fitting of the measured *FWHM* at 5.9 keV as a function of shaping time at –5 V reverse bias (Fig. 14) and can be seen in Fig. 17 as a function of temperature for both S1 and S2. This total leakage current includes twice the contribution of the detector leakage current, I_R, and the input JFET leakage current.[34,39] The leakage current of the input JFET for the currently reported configuration, where the gate of the JFET is slightly forward biased,[30] equals the drain to gate leakage current, I_{DG}.[34] The total leakage current, i.e., $2(I_R + I_{DG})$, was found to decrease from 409 pA at 80 °C to 23 pA at –20 °C for S1, and from 828 pA at 80 °C to 16 pA at –20 °C for S2. The leakage current of an n-type channel JFET, I_{DG}, is a function of its operating point, V_{DS} (drain to source potential difference), and equally, of the drain to gate potential difference, V_{DG}, since the source is grounded. As the drain to gate potential difference is

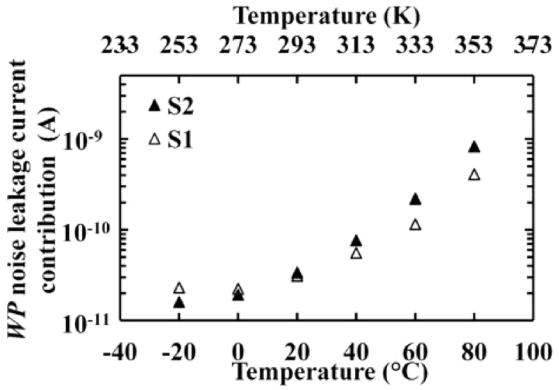

FIG. 17. Total leakage current contribution to the white parallel noise for the GaAs p^+-i-n^+ mesa photodiode based spectrometer S1 (open triangles) and S2 (filled triangles) as a function of temperature, as deduced from multi-dimensional least squares fitting of the measured *FWHM* at 5.9 keV as a function of shaping time, at –5 V reverse bias.

increased, the leakage current of the reverse biased drain to gate junction also increases. The leakage current of the detector, I_R, and the drain to gate potential difference, V_{DG}, are inversely proportional. Consequently, a reduced detector leakage current results in an increased JFET leakage current, I_{DG}. This is in accordance with the findings presented in Fig. 17. The total leakage current of the spectrometer S2 was found to be higher than that of the spectrometer S1 at temperatures ≥20 °C, which was attributed to the detector leakage current, I_R, (∼1 pA to ∼100 pA at -5 C reverse bias) dominating over the JFET leakage current in the corresponding temperature range and to the higher leakage current of D2 than D1 (Fig. 4). However, the total leakage current of S2 was found to be lower than that of the S1 at temperatures ≤0 °C. At this low temperature range, both diodes D1 and D2 had leakage currents of <1 pA at –5 V reverse bias, which are believed to give rise to an increased non-negligible JFET leakage current, I_{DG}.

The thicker i layer of the presently reported devices, compared to previously reported thinner GaAs p^+-i-n^+ mesa photodiodes,[15–18] resulted in higher quantum detection efficiency and improved energy resolution at the investigated temperature range. The improved energy resolution of the presently reported spectrometer was attributed to the reduced white series, 1/*f*, and dielectric noise, all depending upon the capacitance of the photodiode. However, the better energy resolution (*FWHM* at 5.9 keV) achieved at 60 °C with a spectrometer employing a 7 μm i layer thickness GaAs p^+-i-n^+ mesa photodiode (0.84 keV),[18] compared to the currently reported 10 μm i layer thickness GaAs p^+-i-n^+ mesa photodiode, D1, (0.92 keV) was attributed to the lower leakage current of the 7 μm i layer device (27 pA) compared to that of D1 (43 pA), in the specific operating conditions. The dielectric noise, which was found to decrease from 1.13 keV at 80 °C to 0.59 keV at –20 °C for S1, and from 1.50 keV at 80 °C to 0.64 keV at –20 °C for S2, was the dominant source of noise in the temperature range 80 °C to –20 °C, at all investigated shaping times, at –5 V reverse bias, apart from shaping times ≥3 μs at 80 °C, ≥6 μs at 60 °C, and = 10 μs at 40 °C, where the parallel white noise dominated. This resulted in an energy resolution not as good as the best results achieved with GaAs p^+-i-n^+ diodes with Schottky contacts and guard rings at room temperature (0.266 keV *FWHM* at 5.9 keV[12] and 0.300 keV *FWHM* at 5.9 keV[14]). The dielectric noise was minimised in the detector-preamplifier system reported by Owens *et al.*[12] and Erd *et al.*[14] by mounting both the detector and input JFET of the preamplifier in close proximity on the same low-loss substrate. It was estimated that if the dielectric noise of the additional dielectrics could be eliminated from the presently reported system, the energy resolution (*FWHM* at 5.9 keV) at 20 °C of both spectrometers S1 and S2 would be reduced to 0.400 keV, respectively.

V. CONCLUSION

Two fully etched GaAs p^+-i-n^+ mesa X-ray photodiodes, D1 (200 μm diameter) and D2 (400 μm diameter), have been characterized for their electrical and photon counting X-ray spectroscopic performance within the temperature range 100 °C to –20 °C.

The ideality factor improved from (1.91 ± 0.02) at –20 °C to (1.84 ± 0.02) at 0 °C and remained stable, within uncertainties, up to 100 °C for D1, and from (1.90 ± 0.01) at –20 °C to (1.86 ± 0.02) at 20 °C and remained stable, within uncertainties, up to 100 °C for D2. This indicated that the recombination current defined the forward current within the investigated temperature range, with an increased diffusion current contribution at temperatures ≥0 °C and ≥20 °C for D1 and D2, respectively, compared to lower temperatures. The leakage current of both diodes, being comparable to other high quality GaAs p^+-i-n^+ diodes, was found to not scale with area, suggesting that the surface component was not negligible. At the highest investigated reverse bias, –50 V (50 kV/cm internal electric field), the leakage current was found to decrease from 1.615 nA ± 0.007 nA at 100 °C to a current (0.1 pA) smaller than its uncertainty associated with the measurement (±0.4 pA) at –20 °C for D1, and from 2.43 nA ± 0.01 nA at 100 °C to a current (0.2 pA) smaller than its uncertainty associated with the measurement (±0.4 pA) at –20 °C for D2. The logarithm of leakage current density, $\ln(J_R)$, at 50 kV/cm as a function of $1/kT$ graph for both D1 and D2, had gradients equal to equal $-E_G/2$ (–0.74 eV ± 0.3 eV for D1 and –0.75 eV ± 0.2 eV for D2), suggesting that generation was the prevailing conduction process.

Both the diffusion capacitance and the depletion layer capacitance of the diodes D1 and D2, with the packaging capacitance excluded, was found to be temperature-dependent at the investigated temperature range. The diffusion capacitance at 1 V forward bias decreased from 4.368 pF ± 0.008 pF at 100 °C to 1.806 pF ± 0.006 pF at –20 °C for D1, and from 9.679 pF ± 0.014 pF at 100 °C to 4.765 pF ± 0.009 pF at –20 °C for D2, following the forward current decrease with temperature. The depletion layer capacitance at –50 V reverse bias decreased from 0.344 pF ± 0.005 pF at 100 °C to 0.334 pF ± 0.005 pF at –20 °C for D1, and from 1.416 pF ± 0.006 pF at 100 °C to 1.396 pF ± 0.006 pF at –20 °C for D2. Both diodes were

found to be almost fully depleted even with no applied bias; their depletion width was found to increase with decreased temperature; it increased from $9.2\,\mu m \pm 0.1\,\mu m$ at 100 °C to $10.0\,\mu m \pm 0.1\,\mu m$ at –20 °C for D1, and from $9.10\,\mu m \pm 0.03\,\mu m$ at 100 °C to $9.76\,\mu m \pm 0.04\,\mu m$ at –20 °C) for D2, at zero applied bias. The effective doping concentration within the i layer was $8.2 \times 10^{13}\,cm^{-3}$ and $1.22 \times 10^{14}\,cm^{-3}$ at the highest investigated temperature, 100 °C, for D1 and D2, respectively.

The best energy resolution (*FWHM* at 5.9 keV) achieved with the spectrometer S1 (employing D1) and spectrometer S2 (employing D2) was temperature-dependent; the achieved *FWHM* decreased from 2.00 keV at 100 °C to 0.66 keV at –20° C for S1, and from 2.71 keV at 100 °C to 0.71 keV at –20 °C for S2. The noise analysis at –5 V reverse bias within the temperature range 80 °C to –20 °C revealed the dominant source of noise at each temperature and shaping time of each spectrometer; the dielectric noise was the dominant source of noise at all investigated temperatures and shaping times apart from shaping times $\geq 3\ \mu s$ at 80 °C, $\geq 6\ \mu s$ at 60 °C, and $= 10\ \mu s$ at 40 °C, where the parallel white noise dominated. The multidimensional least squares fitting of the measured *FWHM* at 5.9 keV as a function of temperature and shaping time, at –5 V reverse bias allowed the determination of the dielectric noise, and the leakage current, $2(I_R + I_{DG})$, being present in each spectrometer. The dielectric noise decreased from 1.13 keV at 80 °C to 0.59 keV at –20 °C for S1, and from 1.50 keV at 80 °C to 0.64 keV at –20 °C for S2. The apparent total leakage current, $2(I_R + I_{DG})$), decreased from 409 pA at 80 °C to 23 pA at –20 °C for S1, and from 828 pA at 80 °C to 16 pA at –20 °C for S2.

Although the spectrometers S1 and S2, employing the diodes, D1 and D2, respectively, had better energy resolution (*FWHM* at 5.9 keV) compared to previously reported thinner GaAs p^+-i-n^+ mesa X-ray photodiodes,[15–18] further work is required to improve the *FWHM* to values close to the best results achieved with planar Schottky contact GaAs X-ray detectors at room temperature; 0.266 keV *FWHM* at 5.9 keV[12] and 0.300 keV *FWHM* at 5.9 keV.[14] Thicker devices would result in a lower capacitance, which has a direct effect in reducing the white series, 1/*f*, and dielectric noises. Also, future device passivation may reduce the surface component of the leakage current and its parallel white noise contribution, improving the X-ray performance of the devices. Part of the future work is also the novel redesign of the preamplifier front-end by integrating the detector with the input JFET in the same low-loss substrate, which is believed to reduce the dielectric noise.[37] Alternatively, an ASIC preamplifier could also be considered to advance the noise performance of the reported spectrometers, due to its noise level being of a few e^- rms.[41]

ACKNOWLEDGMENTS

This work was in part supported by the Science and Technologies Facilities Council, United Kingdom, through Grant Nos. ST/M004635/1 and ST/P001815/1 (A.M.B., PI). A.M.B. acknowledges funding from the Leverhulme Trust, United Kingdom, in the form of a 2016 Philip Leverhulme Prize. The authors are grateful to B. Harrison, R. J. Airey, and S. Kumar at the EPSRC National Epitaxy Facility for material growth and device fabrication. M.D.C.W. acknowledges funding received in the form of a Ph.D. scholarship from University of Sussex, UK. Data underlying this work are subject to commercial confidentiality. The Authors regret that they cannot grant public requests for further access to any data produced during the study, however the key findings are fully included within the article.

[1]G. Bertuccio and D. Maiocchi, J. Appl. Phys. **92**, 1248 (2002).
[2]C. Hu, *Modern Semiconductor Devices for Integrated Circuits* (Prentice Hall, New Jersey, 2010).
[3]G. Bertuccio, Nucl. Instrum. Methods A **546**, 232 (2005).
[4]G. Bertuccio, C. Canali, and F. Nava, Nucl. Instrum. Methods A **410**, 29 (1998).
[5]B. L. Henke, E. M. Gullikson, and J. C. Davis, At. Data Nucl. Data Tables **54**, 181 (1993).
[6]T. Ly Anh, A. Perd'ochová, V. Nečas, and V. Pavlicová, Nucl. Phys. B (Proc. Suppl.) **150**, 402 (2006).
[7]V. K. Dixit, S. K. Khamari, S. Manwani, S. Porwal, K. Alexander, T. K. Sharma, S. Kher, and S. M. Oak, Nucl. Instrum. Methods A **785**, 93 (2015).
[8]M. Ladzianský, A. Šagátová, V. Nečas, F. Dubecký, and V. Linhart, Nucl. Instrum. Methods A **607**, 135 (2009).
[9]A. Šagátová, B. Zat'ko, M. Pavlovič, K. Sedlačková, P. Hybler, F. Dubecký, and V. Nečas, J. Instrum. **9**, C04036 (2014).
[10]G. P. Summers, E. A. Burke, P. Shapiro, S. R. Messenger, and R. J. Walters, IEEE Trans. Nucl. Sci. **40**, 1372 (1993).
[11]L. Rossi, P. Fischer, T. Rohe, and N. Wermes, *Pixel Detectors: From Fundamentals to Applications* (Springer, Heidelberg, Berlin, 2006).
[12]A. Owens, M. Bavdaz, A. Peacock, A. Poelaert, H. Andersson, S. Nenonen, H. Sipila, L. Tröger, and G. Bertuccio, J. Appl. Phys. **90**, 5376 (2001).
[13]A. Owens, M. Bavdaz, A. Peacock, A. Poelaert, H. Andersson, S. Nenonen, L. Tröger, and G. Bertuccio, Nucl. Instrum. Methods A **466**, 168 (2001).
[14]C. Erd, A. Owens, G. Brammertz, M. Bavdaz, A. Peacock, V. Lämsä, S. Nenonen, H. Andersson, and N. Haack, Nucl. Instrum. Methods A **487**, 78 (2002).
[15]A. M. Barnett, J. E. Lees, D. J. Bassford, J. S. Ng, C. H. Tan, N. Babazadeh, and R. B. Gomes, Nucl. Instrum. Methods A **654**, 336 (2011).
[16]A. M. Barnett, Nucl. Instrum. Methods A **756**, 39 (2014).
[17]J. S. Ng, X. Meng, J. E. Lees, A. M. Barnett, and C. H. Tan, J. Instrum. **9**, T08005 (2014).
[18]G. Lioliou, X. Meng, J. S. Ng, and A. M. Barnett, J. Appl. Phys. **119**, 124507 (2016).
[19]G. Lioliou and A. M. Barnett, Nucl. Instrum. Methods A **836**, 37 (2016).
[20]S. M. Sze, *Physics of Semiconductor Devices*, 3rd ed. (John Wiley and Sons, New Jersey, 2007).
[21]A. Sellai, in *Proceedings of the IEEE International Conference on Semiconductor Electronics*, edited by S. Shaari, Johor, Malaysia, 25–27 November (2008), pp. 267–270.
[22]M. S. Carpenter, M. R. Melloch, M. S. Lundstrom, and S. P. Tobin, Appl. Phys. Lett. **52**, 2157 (1988).
[23]W. Wang, G. Lee, M. Huang, R. M. Wallace, and K. Cho, J. Appl. Phys. **107**, 103720 (2010).
[24]M. T. Sheldon, C. N. Eisler, and H. A. Atwater, Adv. Energy Mater. **2**, 339 (2012).
[25]G. Bertuccio, R. Casiraghi, D. Maiocchi, A. Owens, M. Bavdaz, A. Peacock, H. Andersson, and S. Nenonen, IEEE Trans. Nucl. Sci. **50**, 723 (2003).
[26]M. Mazzillo, A. Sciuto, G. Catania, F. Roccaforte, and V. Raineri, IEEE Sens. J. **12**, 1127 (2012).
[27]J. F. White, *Microwave Semiconductor Engineering* (Springer, The Netherlands, 1982).
[28]D. Schroder, *Semiconductor Material and Device Characterization* (John Wiley and Sons, New Jersey, 2006).

[29]R. A. Stradling and P. C. Klipstein, *Growth and Characterisation of Semiconductors* (IOP Publishing, Ltd., England, 1990).
[30]G. Bertuccio, P. Rehak, and D. Xi, Nucl. Instrum. Methods A **326**, 71 (1993).
[31]*N-Channel JFETs* (Vishay Intertechnology, Inc., USA, 2005), p. 2N4416.
[32]U. Schötzig, Appl. Radiat. Isot. **53**, 469 (2000).
[33]M. Sánchez del Rio, A. Brunetti, B. Golosio, A. Somogyi, and A. Simionovici, *XRAYLIB Tables (X-Ray Fluorescence Cross-Section)* (European Synchrotron Radiation Facility and University of Sassari, 2003).
[34]G. Lioliou and A. M. Barnett, Nucl. Instrum. Methods A **801**, 63 (2015).
[35]G. Bertuccio, A. Pullia, J. Lauter, A. Forster, and H. Luth, IEEE Trans. Nucl. Sci. **44**, 1 (1997).
[36]A. Owens, *Compound Semiconductor Radiation Detectors* (CRC Press, Florida, 2012).
[37]G. Bertuccio and A. Pullia, Rev. Sci. Instrum. **64**, 3294 (1993).
[38]G. Bertuccio, A. Pullia, and G. De Geromino, Nucl. Instrum. Methods A **380**, 301 (1996).
[39]G. Bertuccio and R. Casiraghi, IEEE Trans. Nucl. Sci. **50**, 175 (2003).
[40]J. Krupka, D. Mouneyrac, J. G. Hartnett, and M. E. Tobar, IEEE Trans. Microwave Theory Technol. **56**, 1201 (2008).
[41]G. Bertuccio and S. Caccia, Nucl. Instrum. Methods A **579**, 243 (2007).